HOKKAIDO UNIVERSITY

Title	Cracking and Chemical Composition of Cement Paste Subjected to Heating and Water Re-Curing
Author(s)	Henry, Michael; Hashimoto, Katsufumi; Darma, Ivan Sandi et al.
Citation	Journal of advanced concrete technology, 14(4), 134-143 https://doi.org/10.3151/jact.14.134
Issue Date	2016-04
Doc URL	https://hdl.handle.net/2115/63007
Rights(URL)	https://creativecommons.org/licenses/by/2.0/
Type	journal article
File Information	14_134.pdf

Hokkaido University Collection of Scholarly and Academic Papers : HUSCAP

Journal of Advanced Concrete Technology
Materials, Structures and Environment

Cracking and chemical composition of cement paste subjected to heating and water re-curing

Michael Henry, Katsufumi Hashimoto, Ivan Sandi Darma, Takafumi Sugiyama

Journal of Advanced Concrete Technology, volume 14 (2016), pp. 134-143

Related Papers Click to Download full PDF!

Transport Properties of Fire-Exposed Concrete
Wilasa Vichit-Vadakan, Elizabeth A. Kerr
Journal of Advanced Concrete Technology, volume 7 (2009), pp. 393-401

X-ray microtomography of mortars exposed to freezing-thawing action
Michael A. B. Promentilla, Takafumi Sugiyama
Journal of Advanced Concrete Technology, volume 8 (2010), pp. 97-111

Application of X-ray CT to study diffusivity in cracked concrete through the observation of tracer transport
Ivan Sandi Darma, Takafumi Sugiyama, Michael A. B. Promentilla
Journal of Advanced Concrete Technology, volume 11 (2013), pp. 266-281

Click to Submit your Papers
Japan Concrete Institute http://www.j-act.org

Scientific paper

Cracking and Chemical Composition of Cement Paste Subjected to Heating and Water Re-Curing

Michael Henry[1*], Katsufumi Hashimoto[2], Ivan Sandi Darma[3] and Takafumi Sugiyama[4]

Received 7 January 2016, accepted 2 April 2016 doi:10.3151/jact.14.134

Abstract

Water re-curing of fire-damaged concrete may reduce the environmental and economic impacts of repair operations by re-using the existing concrete. To clarify the rehydration mechanism, the effects of water re-curing on the microstructure and chemical properties of fire-damaged cement paste were examined. Analysis by X-ray CT showed that heating led to radial cracks that propagated horizontally and vertically in the cement paste specimen. Water supply led to a growth in the cracked space through an increase in the connectivity of the crack network. This growth may be due to expansion caused by the rehydration of CaO into $Ca(OH)_2$. Chemical analyses suggest that the rehydration reaction differs from the initial hydration in that C_2S plays a greater role in generating C-S-H gel during the earlier period of water re-curing.

1. Introduction

Concrete exposed to high temperatures may suffer a deterioration of its integrity and physical properties. This deterioration is driven by a variety of physical and chemical reactions (Taylor 1997). Evaporation of free water proceeds between 30ºC and 100ºC, followed by the loss of chemically-bound water in the C-S-H and carboaluminate hydrates between 180ºC and 300ºC. From 450ºC to 550ºC, dehydration of calcium hydroxide occurs, producing calcium oxide. Finally, decomposition of calcium carbonate and C-S-H gel begins between 600ºC and 700ºC. These reactions cause the pore structure to coarsen and the formation of cracks both at the surface and internally due to shrinkage of the concrete and incompatibility in the thermal expansion between the aggregates and the mortar.

As a result, concrete structures subjected to fire suffer reduced load-carrying capacity, durability, and fire resistance, and may require repair or strengthening operations to restore safety. Repair of damaged areas involves the removal of the surface concrete, preparation of the exposed surfaces, and casting of a patching material (Tovey 1986). Unfortunately, the removal and preparation processes require intense labor and energy and produce waste material that must be disposed of, while replacing the damaged areas consumes natural resources. A repair method that re-uses the existing concrete could provide a more economical and environmentally friendly repair option.

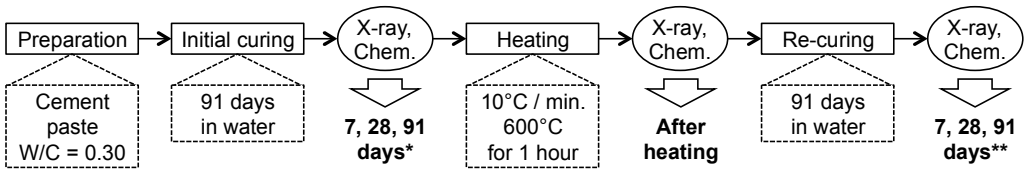
Past research works have shown that re-curing fire-damaged concrete in water or a high humidity environment can lead to performance recovery. It has been suggested that rehydration of the dehydrated gel, hydration of previously unhydrated cement grains, and the carbonation of calcium oxide all contribute to performance recovery through the reduction of pore space and the healing of cracks (Crook and Murray 1970; Khoury 1992; Sarshar and Khoury 1993; Lin *et al*. 1996; Henry *et al*. 2014), although the instability of healed crack areas may limit the strength recovery (Henry *et al*. 2011). While carbonation of calcium oxide can increase strength, it may reduce long-term durability in reinforced concrete due to carbonation-induced corrosion (Taylor 1997); however, water re-curing can consume the calcium oxide used in the carbonation reaction and reduce the carbonation effect (Henry *et al*. 2011). On the other hand, the effect of the rehydration of calcium oxide into calcium hydroxide is unclear, as it has been reported that the volume increase that accompanies this reaction may actually reduce performance through the growth of cracks (Petzold and Rohrs 1970), whereas other research has suggested that the reaction is important for performance recovery (Poon *et al*. 2001).

The aim of this study is to examine the rehydration reaction and its effects on the physical structure of fire-damaged cementitious materials under water re-curing, and to obtain qualitative and quantitative data for assessing the efficacy of water re-curing as a repair method for fire-damaged concrete structures. X-ray microtomography was utilized to characterize the forma-

[1]Assistant professor, Division of Field Engineering for the Environment, Faculty of Engineering, Hokkaido University, Sapporo, Japan. *Corresponding author: *E-mail:* mwhenry@eng.hokudai.ac.jp
[2]Assistant professor, Division of Engineering and Policy for Sustainable Environment, Faculty of Engineering, Hokkaido University, Sapporo, Japan.
[3](former) Ph.D. student, Division of Field Engineering for the Environment, Graduate School of Engineering, Hokkaido University, Japan.
[4]Professor, Division of Field Engineering for the Environment, Faculty of Engineering, Hokkaido University, Sapporo, Japan.

Table 1 Chemical composition of OPC (% weight of powder).

SiO_2	Al_2O_3	Fe_2O_3	CaO	MgO	SO_3	Na_2O	K_2O	MnO	TiO_2	C_3S	C_2S	C_3A	C_4AF
21.9	5.2	3.1	64.4	1.4	1.7	0.2	0.4	0.3	0.3	56	18	9	9



** X-ray CT at 91 days (before heating) only*
*** X-ray CT at 28 and 91 days only*

Fig. 1 Overview of experimental program.

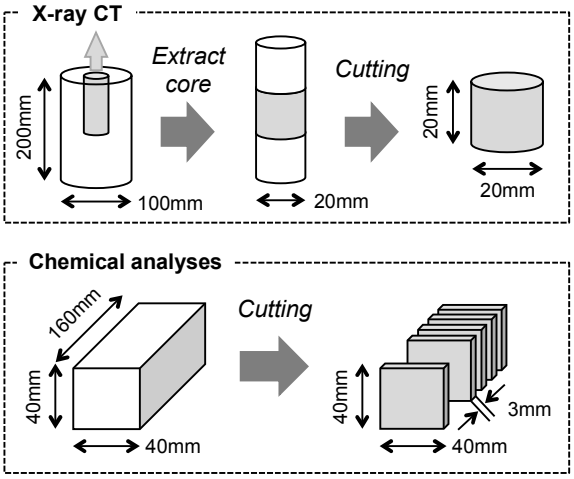


Fig. 2 Preparation processes for X-ray CT and chemical analyses specimens.

tion and propagation of cracks under heating and re-curing, and chemical analyses were conducted to evaluate the hydration and re-hydration reactions during initial curing and post-heating water re-curing, respectively. The results from these two approaches were then synthesized to better understand the behavior of cementitious materials when subjected to water re-curing after high temperature exposure.

2. Experimental program

An overview of the experimental program is shown in **Fig. 1**.

2.1 Specimen preparation and initial curing

Cement paste was prepared with a water-cement ratio (W/C, by mass) of 0.30 using ordinary Portland cement (OPC, density: 3.16 g/cm^3, specific surface area: 3320 cm^2/g) and tap water. The chemical composition of OPC is shown in **Table 1**. Cylinder (Φ100 x 200 mm) and beam (40 x 40 x 160 mm) specimens were cast, sealed, and cured in the molds for 24 hours, then removed and placed in water curing at 20°C. The preparation processes for the X-ray CT and chemical analysis specimens are shown in **Fig. 2**. For X-ray CT imaging, the cylinder was cured in the water for 28 days, after which it was removed and a 20 mm diameter core was extracted from the center of the cylinder. A segment 20 mm in length was cut from this core, after which the segment was returned to water curing for another 63 days. For the chemical analyses, the beam was also cured in the water for 28 days before removal and cutting into slices (40 x 40 x 3 mm), except in the case of the chemical analyses conducted at 7 days initial curing; in this case, slices were cut from the beam after 7 days of water curing. The slices cut at 28 days were returned to water curing for another 63 days. In both cases, in order to achieve a high degree of hydration, the total curing time from casting to heating was 91 days.

2.2 Heating and re-curing

Fire exposure was simulated using an electric furnace with a temperature control program. The rate of heat increase was set at 10ºC per minute until the target exposure temperature of 600ºC was reached. This temperature was selected as it enabled the examination of the case in which high degrees of both dehydration and rehydration would occur. The target temperature was maintained for one hour, after which the furnace was turned off and the door of the furnace opened. Specimens were allowed to cool in the furnace until the internal furnace temperature dropped below 100ºC, then were removed from the furnace and cooled at room temperature for approximately one hour before being transferred to water re-curing, the conditions of which were similar to the initial curing period. Re-curing was carried out for a period of up to 91 days.

2.3 X-ray CT and image analyses

X-ray computed tomography (CT) provides a non-destructive means of examining the internal structure of an object in three dimensions and, when combined with image analysis techniques, can enable the quantitative evaluation of an object's internal structure. As summarized by Promentilla and Sugiyama (2010) and Landis and Keane (2010), using X-ray CT, a 3D digital image can be reconstructed from a series of 2D images, or "slices." Each voxel (3D pixel) within the 3D digital image has an X-ray absorption value that can be correlated to material density, and thus the internal structure can be determined based on the arrangement of the vox-

Table 2 Image acquisition settings.

Test series	FID (mm)	FCD (mm)	Slice thickness (μm)	Pixel size (μm)	No. slices in stack
Before heating	600	170	33.0	21.2	351
After heating	600	170	33.0	21.2	351
28 days re-curing	600	170	33.0	21.2	351
91 days re-curing	600	180	34.3	22.8	351

FID: focus image distance; FCD: focus chamber distance

els in a 3D space. Images are constructed on a grey scale from 0 (black) to 255 (white). The grey scale value (GSV) is calculated from the CT value, which in turn is based on the X-ray absorption coefficient of a material. The GSV can thus be considered a representation of material density, where lighter shades represent higher density and darker shades lower density.

As reported by Henry *et al*. (2014), this research used a desktop microfocus CT system, which consists of a microfocus X-ray emitter, a rotation table, an image intensifier detector with CCD camera, and an image processing unit. The focus area was approximately 11.5 mm in height and roughly centered on the specimen, as shown in **Fig. 3**. The image acquisition conditions are given in **Table 2**. Each slice was 1024 by 1024 pixels in size. Imaging was carried out on a single specimen before heating (91 days initial curing), after heating, and after 28 and 91 days of water re-curing. As the specimen had to be removed in between scans for heating and re-curing, measures were taken to keep the specimen centered on the table and to maintain the same orientation.

In order to extract and quantitatively evaluate the cracked space in the specimen, image analysis techniques were employed (Henry *et al*. 2014). Threshold segmentation and multiple cluster labeling were respectively applied to isolate the total void space from the cement paste and to separate the connected void space (i.e., cracks) from the isolated void space. The method is illustrated in **Fig. 4**. First, the total void space could be

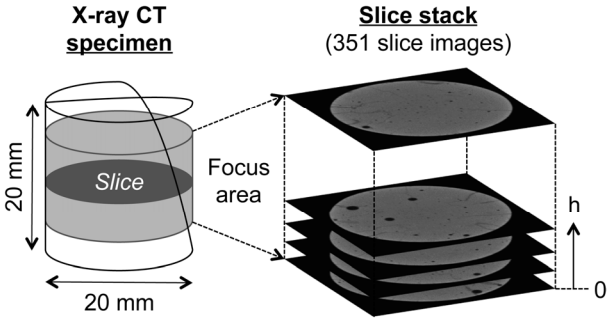
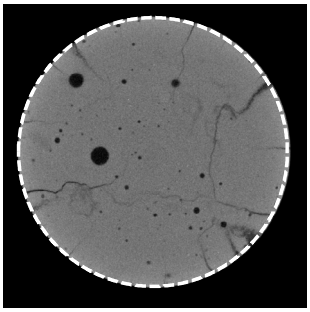
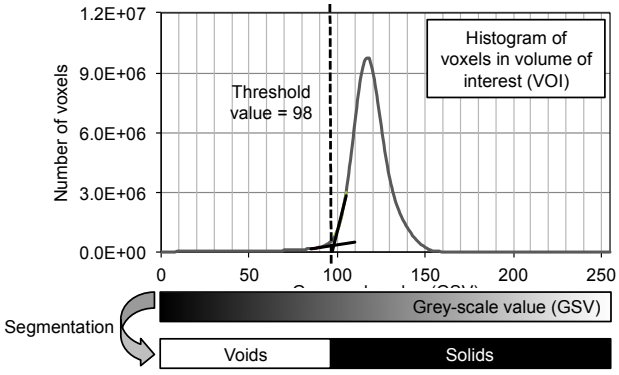


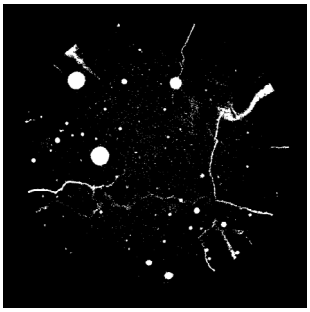
Fig. 3 Image acquisition area in X-ray CT specimen.



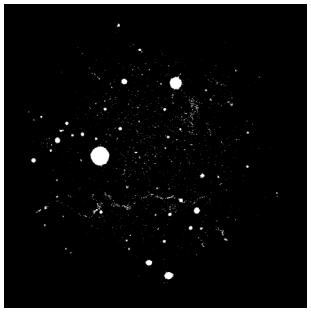
(1) Original grey-scale image with region of interest (ROI) indicated by dashed line



(2) Establishment of threshold based on GSV distribution and re-labeling of voxels to identify void and solid spaces



(3) Segmented image showing total void space



(4) Isolated voids identified by connectivity analysis



(5) Isolated voids removed from (3) and connected void space (crack) extracted

Fig. 4 Method for extracting total void space and identifying connected voids.

extracted from the volume of interest (VOI, the region of interest (ROI) across the vertical slice stack) by selecting a threshold value from the grey-scale value histogram, and using that value to convert the grey-scale images to binary black and white that correspond to solid and void space, respectively (Promentilla *et al*. 2008; Darma *et al*. 2013).

Next, following the methodology of Hoshen and Kopelman (1976) and Ikeda *et al*. (2000), the connected crack space could be extracted by carrying out cluster multiple labeling (connectively analysis) on the void space, which identified connected voids using connectivity rules in which two voxels can be labeled as "connected" if they share a common face with each other (**Fig. 5**). A group of connected voxels is called a cluster, and can be quantified by the number of voxels, their relative position in a 3D space, and the voxel size. In this study, the largest connected void cluster was treated as the connected crack space, while the other void clusters were treated as isolated void space. Total, isolated, and connected void space volumes were then calculated as a percentage of the total volume of the VOI.

2.4 Chemical analyses

Chemical analyses were carried out using powder obtained from crushing and grinding slice specimens after 7, 28, and 91 days of initial water curing; after heating; and after 7, 28, and 91 days of water re-curing.

TG-DTA (Thermo-gravimetric Differential Thermal Analysis) was used to evaluate the changes in hydration products. A heating speed of 10°C per minute and a maximum temperature of 1000°C were set as the measurement conditions, and two properties of the cement paste were targeted: the amount of calcium hydroxide ($Ca(OH)_2$), which was calculated by the mass change that occurred at approximately 450°C, and the amount of chemically-bound water, which was measured by the ignition loss between 105°C and 1000°C. The reported results are the average of two tests per time point.

XRD (X-ray diffraction) was used to evaluate the changes in the crystalline structure of the cement paste. The scanning range was 2θ = 5 to 60 degrees with a 0.02 step scan and a scanning speed of 5.5 degrees per minute. The diffraction profile was acquired using powder diffraction analysis software, and analysis targeted the diffraction peaks of alite (C_3S), belite (C_2S), calcium aluminate (C_3A), and calcium hydroxide. Measurements were carried out twice at each time point, but only a single set of XRD curves is reported, as little difference was observed between the two results.

3. Results

3.1 Cross-sectional images of cement paste specimens

The internal conditions of the specimens before and after heating are first examined using non-segmented cross-sectional images (**Fig. 6**). As the specimen consists primarily of two phases – cement paste and air – the images are mainly two-tone, with light grey indicating the cement paste and the black areas representing voids. Images taken before heating show no cracking, but voids (entrained or entrapped air) can be observed inside the specimen. Some cracking can be observed after heating, and these cracks appear to grow larger as water re-curing progressed, but it is difficult to fully grasp the cracking behavior from the cross-sectional images alone. Therefore, the previously introduced segmentation and connectivity analysis methods were applied to extract and quantitatively evaluate the connected crack space.

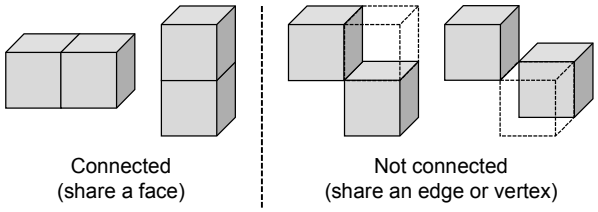


Fig. 5 Definition of connectivity for adjacent voxels in connectivity analysis.

3.2 Crack generation and propagation behavior

Figure 7 shows the cross-sectional images of the extracted cracks after heating and after 28 and 91 days of water re-curing. The segmented images for before heating are not included, as no connected crack space was found in this case. After heating, some small cracks were identified. They appeared to propagate radially and, in some cases, intersect air voids in the specimen. After 28 days of water re-curing, however, many of the microcracks observable after heating grew in size. The connected void space increased significantly from after heating, which suggests that water re-curing led to an increase in the crack space within the specimen. A comparison of images from after 28 and 91 days of water re-curing shows little change under the extended re-curing period.

The 3D crack structure can be reconstructed by stacking the slice images of the crack space to form a 3D volume. The reconstruction for 28 days of water re-curing is shown in **Fig. 8**. By visualizing the crack structure in three dimensions, it can be seen that the cracks propagated radially inwards from the specimen surface, as was seen in the 2D cross-section images, but that the cracks themselves occurred both vertically (in the Z-direction) as well as horizontally (in the X-Y place) to form an inter-connected network. Some of the cracks also intersect air voids in the specimen, which can be clearly seen as large spheres when joined to the connected void space by the propagated cracks.

3.3 Quantification of void space characteristics

Results from the connectivity analysis are summarized in **Table 3**, and the calculated void volumes and connectivity (the ratio of connected to total void space) are

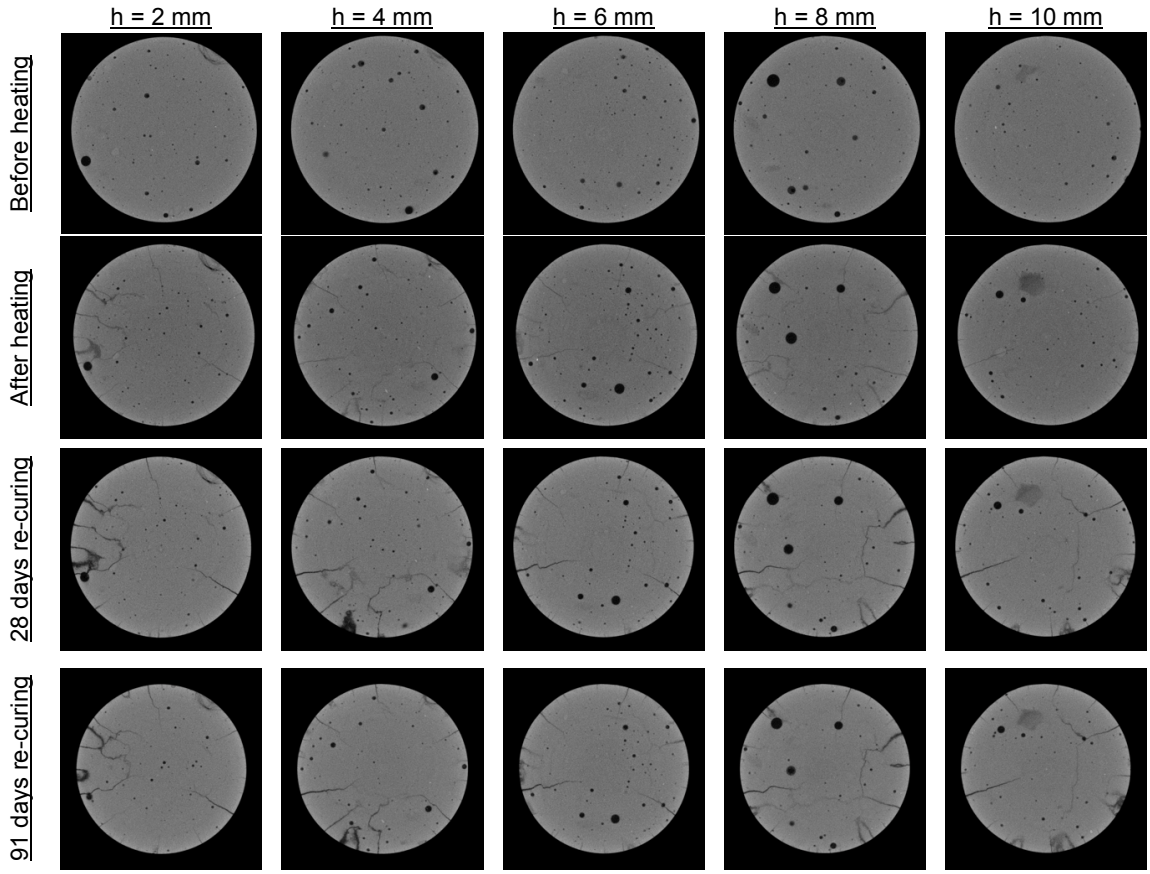


Fig. 6 Non-segmented slice images at selected heights in the focus area.

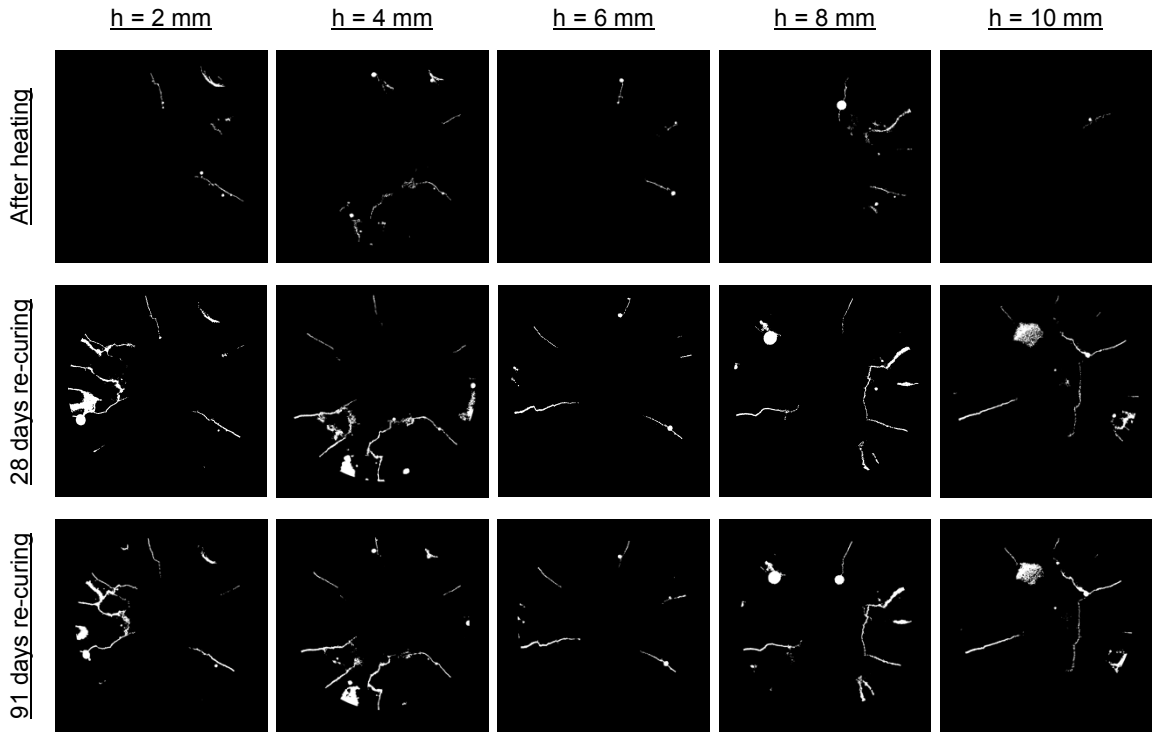
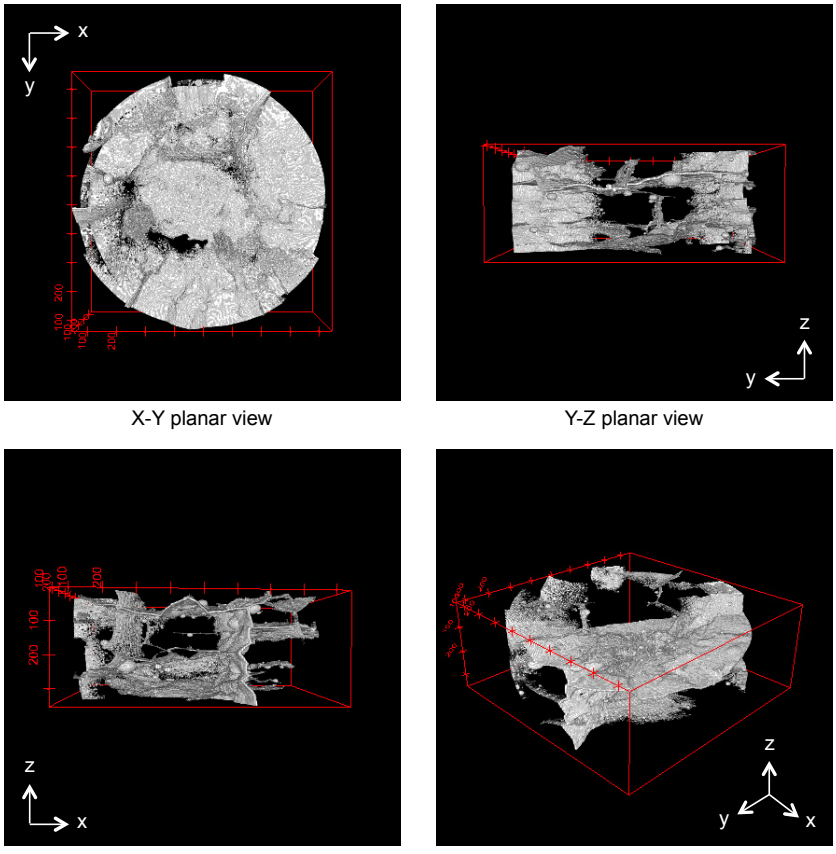


Fig. 7 Connected crack space at selected heights in the focus area.

Table 3 Summary of connectivity analysis results.

	Before heating	After heating	28 days re-curing	91 days re-curing
Total no. voxels in VOI	223,183,350	223,183,350	225,090,900	232,085,250
Total volume (mm^3)	3310.1	3310.1	3401.7	4102.0
Total void space				
No. voxels	7,933,100	10,879,851	9,454,761	9,869,643
Volume (mm^3)	117.7	161.4	142.9	174.4
Connectivity	0.00	13.10	58.32	70.89
Connected void space (largest cluster)				
No. voxels	0	1,424,964	5,513,877	6,995,630
Volume (mm^3)	0.0	21.1	83.3	123.6
Isolated void space				
No. voxels	7,933,100	9,454,887	3,940,884	2,874,013
Volume (mm^3)	117.7	140.2	59.6	50.8



X-Y planar view | Y-Z planar view

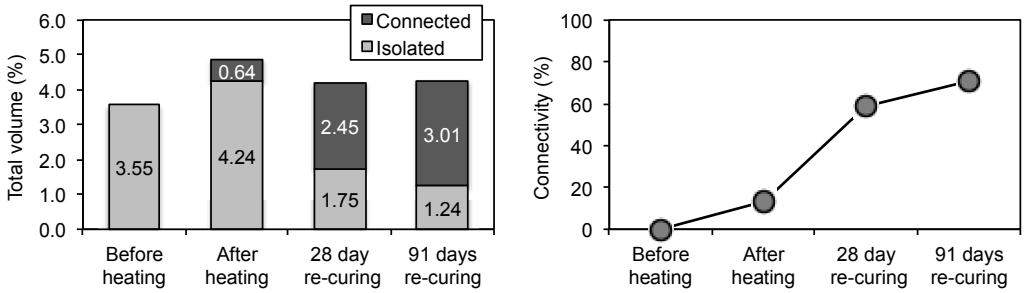
X-Z planar view | Projection view

Fig. 8 Reconstructed 3D crack network after 28 days of water re-curing.

summarized in **Fig. 9**. Before heating, the voids within the specimen were completely isolated. Heating led to an increase in the total void volume, but the connected voids (cracks) made up only 13.1% of the total volume of voids. After water re-curing, however, the total void volume decreased slightly but the connectivity more than quadrupled. This increase in the connected void volume may be attributed to the increase in crack width and crack propagation, which resulted in connecting isolated voids to the connected void space. Extended water re-curing up to 91 days saw little change in the total void volume, but a continued increase in the connectivity. Therefore, crack width growth and crack propagation continued during the latter water re-curing period, although the pace was slower than during the first 28 days.

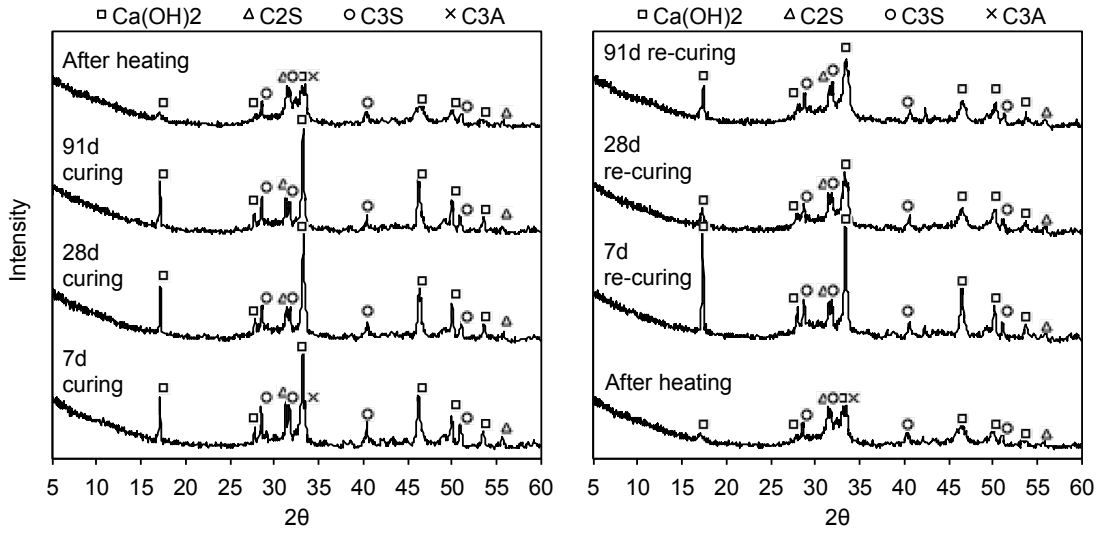
3.4 XRD analysis

Figure 10 shows the XRD curves for the initial curing period, after heating, and the water re-curing period. Peaks corresponding to C_2S and C_3S appear to grow smaller during the initial curing period, although no change is observed after 28 days, and the peak of C_2S is higher than that of C_3S. Prior examination of the anhydrous cement also showed a stronger diffraction signal for C_2S than C_3S. The most noticeable effect of heating



(a) Total, connected, and isolated voids **(b) Connectivity**

Fig. 9 Effect of heating and re-curing on void space characteristics.



(a) Initial curing and after heating **(b) After heating and water re-curing**

Fig. 10 Effect of curing, heating, and re-curing on XRD curves.

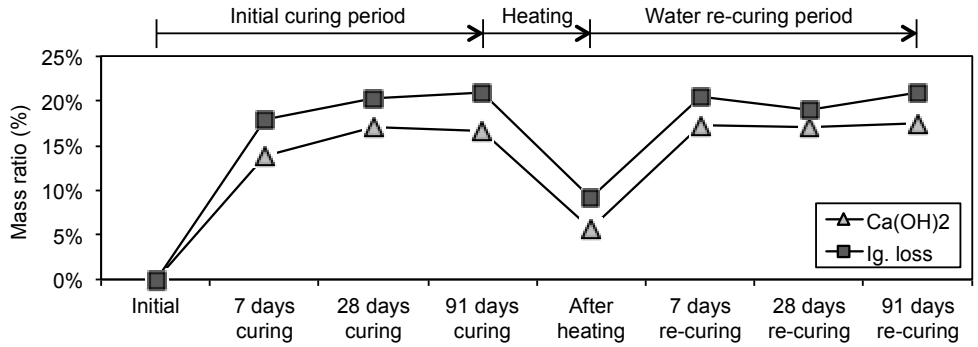


Fig. 11 Effect of curing, heating, and re-curing on calcium hydroxide and ignition loss.

is the reduction in the $Ca(OH)_2$ peaks. The peaks of C_2S and C_3S are smaller after re-curing than during the initial curing period, especially at 28 and 91 days. Additionally, the peaks of C_2S are similar or smaller than the peaks of C_3S.

3.5 TG-DTA analysis

Figure 11 shows the results of the TG-DTA analysis. During the initial curing period, the amounts of calcium hydroxide and chemically bound water undergo their largest increase between 0 and 7 days, but they continue to gradually increase up to 91 days. Heating, however, reduces the amounts of calcium hydroxide and chemically bound water. After re-curing in water for 7 days, the amounts of calcium hydroxide and chemically bound water return to nearly the same level as their pre-fire condition. Unlike the initial curing period, however, little change is observed between 7 and 91 days during the water re-curing period, and the amounts of calcium hydroxide and chemically bound water after 91 days of water re-curing are 104.1% and 99.8%, respectively, of the pre-fire conditions.

To more deeply clarify the re-curing behavior, the normalized mass loss during the TG-DTA testing was

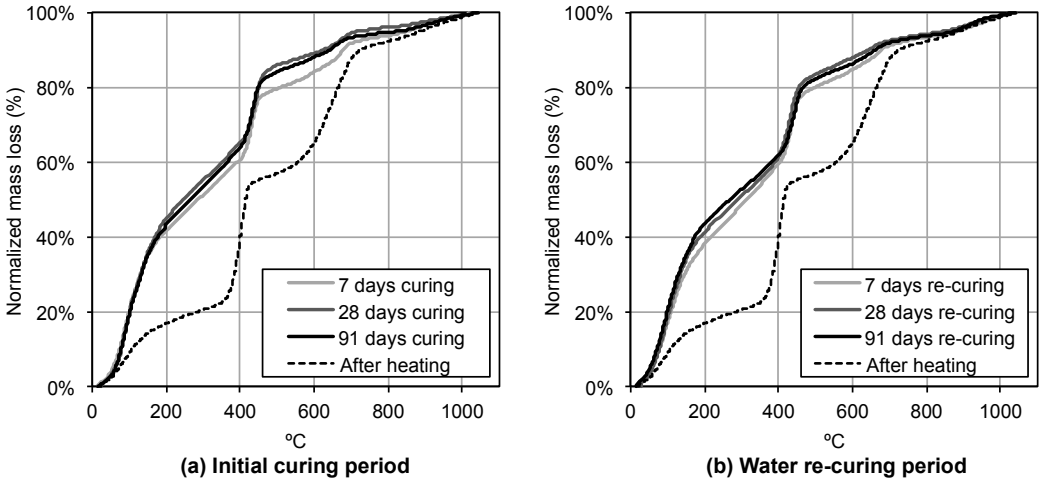
examined for the initial and water re-curing periods (**Fig. 12**). In this figure, the normalized mass loss was calculated as the mass loss at a given temperature during the TG-DTA test as a percentage of the total mass loss of the specimen at the conclusion of the test. Differences in the initial curing and water re-curing periods can be seen for two specific temperature intervals: approximately 200ºC to 400ºC (which corresponds to the presence of C-S-H gel, AFm, and Aft phases) and 400ºC to 700ºC (which corresponds to calcium hydroxide). For the initial curing period, there is little change in the normalized mass loss curves in the lower temperature interval for the period of 7 to 91 days, but a change in the normalized mass loss attributable to calcium hydroxide can be seen to occur in the upper temperature interval between 7 and 91 days. Conversely, little change is seen in the upper temperature interval during the water re-curing period, but a change in the normalized mass loss in the lower temperature interval can be seen from 7 to 91 days. Therefore, while the final observed mass ratios of calcium hydroxide and chemically bound water after 91 days of water re-curing were observed to be relatively the same as before heating, the progression of the rehydration reaction can be said to be different than that of the initial hydration reaction.

4. Discussion

The effect of heating on the physical structure of the cement paste could be clearly seen in the formation of horizontal and vertical cracks, as observed through the X-ray CT images and reconstructed 3D crack network. The generation of these can be attributed to shrinkage of the specimen under the 600ºC heating exposure – a temperature by which thermal expansion is overtaken by shrinkage due to dehydration (Eglinton 1988). Furthermore, the lack of aggregates in the specimen allowed the cracks to propagate radially, in straight, mostly flat planes, inwards from the surface of the specimen. This is in contrast to cracks generated in concrete under heating, which will be more tortuous due to propagation around aggregates present in the matrix (Henry *et al*. 2014). Additionally, in the case of concrete, cracks will also occur in the mortar-aggregate interface due to differences in thermal expansion.

While water re-curing is intended to contribute to performance recovery through, among other factors, crack self-healing, it was observed that the cracks formed post-heating actually grew larger under water re-curing. This crack growth occurred mainly up to 28 days, with little change seen thereafter; this is understandable in light of the limited reactions that were observed up to and after 28 days of re-curing. It is considered that the generation of $Ca(OH)_2$ during rehydration was the main factor driving crack expansion. The rehydration of CaO into $Ca(OH)_2$ is accompanied by an increase in volume, which may contribute to the deterioration of fire-damaged concrete (Petzold and Rohrs 1970). In a previous study using X-ray CT with samples containing aggregates, crack self-healing under water re-curing was observed (Henry *et al*. 2014). In that case, the aggregates served to occupy a large volume of the specimen, thus reducing the relative volume of cement, and also restrained the expansive behavior. Another study using simply high-strength mortar also observed crack self-healing behavior under water supply, which contributed to the recovery of mass transport properties (Henry *et al*. 2011). Conversely, the cement paste specimen examined here was both cement-rich and contained no aggregates, creating a large potential for expansion during water re-curing. The expansive behavior served to connect voids that were previously isolated such that, even though the total void space decreased after 28 days re-curing, the connected void space actually continued to increase up to 91 days. On the one hand, high connectivity is beneficial for performance recovery during early water re-curing, as it allows the rapid supply of water to damaged areas; however, from a durability perspective, in the long term it desirable to reduce connectivity to prevent the ingress of destructive agents.

The re-curing mechanism itself may be explored through the chemical analysis results. A conceptual il-



(a) Initial curing period **(b) Water re-curing period**

Fig. 12 Normalized mass loss for initial curing and water re-curing periods.

lustration of the phase composition during the initial and re-curing periods was constructed based on the chemical analyses (**Fig. 13**). The re-curing reaction is believed to differ from the initial curing in several ways. It has been previously demonstrated that, after 28 days of water re-curing, the amount of $Ca(OH)_2$ can be restored to pre-fire levels in high strength concrete (Henry *et al*. 2011), but the rate of the rehydration reaction relative to the initial reaction was not examined. It was observed in the results here that, although the formation rate of $Ca(OH)_2$ is relatively the same in both reactions, the re-curing reaction begins with an initial amount of $Ca(OH)_2$ present after heating, so it reaches the same value as before heating earlier than the initial curing. Additionally, from 7 days, greater hydration progress for C-S-H during rehydation was observed than in the initial reaction, which was inferred from the change in the 100ºC to 300ºC range of the normalized mass loss during re-curing. Previous research also identified the regeneration of C-S-H under water re-curing as a contributing factor to performance recovery (Sarshar and Khoury 1993), but the results here expand upon that previous study by showing that C-S-H regeneration may have been due to the greater contribution of C_2S to the hydration reaction during re-curing, as C_2S reaction leads to more formation of C-S-H than C_3S.

As cement paste is the material that enables performance recovery of concrete through the rehydration reaction, the results discussed here have implications for the use of water re-curing as a repair method. The observed expansive reaction could have a deleterious effect in concrete, which runs counter to the goal of restoring performance. Concrete using cements that may potentially produce more $Ca(OH)_2$ during rehydration, such as high early strength cement, which contains a greater proportion of C_3S, may be more susceptible to deterioration due to the expansion upon re-curing. Conversely, better performance recovery may occur in concretes with cements that generate more C-S-H, such as low heat of hydration cement, which contains a greater proportion of C_2S. The effect of C_3S and C_2S proportions on the actual concrete performance recovery under water re-curing has not been previously investigated, but it is clear that the recovery potential is dependent on the cement type. While the results discussed here present one step in further understanding the rehydration mechanism, future studies will need to better clarify the role of materials types on the recovery behavior, particularly with regards to the relationship between chemical and mechanical behaviors.

5. Conclusion

In this study, the chemical composition and cracking behavior of cement paste subjected to high temperature exposure and water re-curing were investigated. X-ray CT was utilized to quantitatively evaluate crack formation and propagation, and chemical analyses were applied to compare the rehydration reaction relative to initial hydration. The results were then integrated to clarify the effect of rehydration on the physical structure and identify key points for re-curing as a repair method for fire-damaged concrete. Conclusions are summarized as follows:

1) Comparison of X-ray CT images of the internal microstructure before and after 600ºC heating revealed the formation of radial cracks due to heating. Upon applying image analysis techniques to extract the connected crack structure, it could be seen that crack planes existed both horizontally and vertically in the cement paste specimen. Crack formation could be explained by shrinkage of the specimen under heating due to dehydration of hydration products.
2) Water supply led to a growth in the cracked space through an increase in the connectivity of the crack network, which occurred mostly within the first 28 days of water re-curing. Connectivity of the crack network increased due to crack widening and the formation of bridging cracks due to expansion caused by the rehydration of CaO into $Ca(OH)_2$, the cement-rich composition of the low water-cement ratio specimen, and the lack of aggregates in the matrix to restrain against the expansion reaction.
3) Chemical analyses suggest that the rehydration reaction differs from the initial hydration in two ways. First, the presence of residual $Ca(OH)_2$ at the begin-

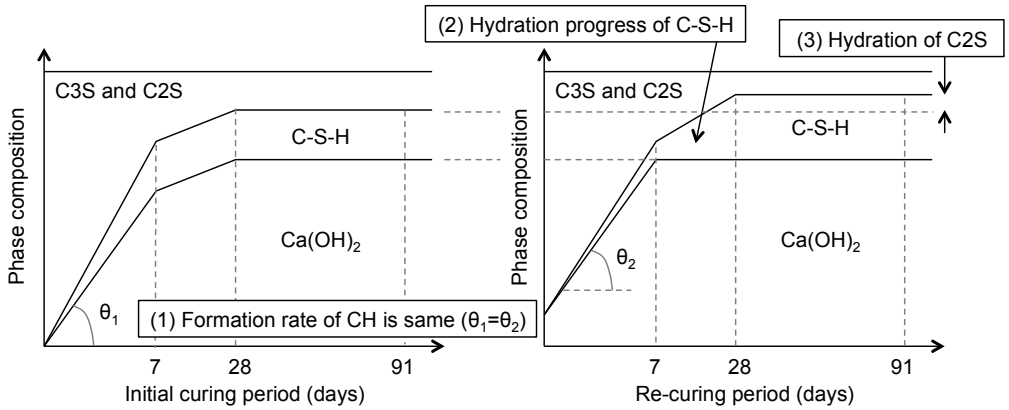


Fig. 13 Differences in phase composition between initial and re-curing periods.

ning of rehydration results in the pre-fire level being reached more quickly than during the initial hydration, with this reaction contributing to the crack expansion during re-curing. Second, C_2S appears to plays a greater role in generating C-S-H gel during the earlier period of water re-curing.

Acknowledgment

This research was partially supported by the Japan Society for the Promotion of Science (JSPS KAKENHI grant number 26289133).

References

Crook, D. N. and Murray, M. J., (1970). "Regain of strength and firing of concrete." *Magazine of Concrete Research*, 22(72), 149-154.

Darma, I. S., Sugiyama, T. and Promentilla, M. A. B., (2013). "Application of X-ray CT to study diffusivity in cracked concrete through the observation of tracer transport." *Journal of Advanced Concrete Technology*, 11, 266-281.

Eglinton, M., (1988). "Resistance of concrete to destructive agencies." In: P. C. Hewlett (Ed.), *Lea's Chemistry of Cement and Concrete* (299-342). Oxford, UK: Elsevier.

Henry, M., Suzuki, M. and Kato, Y., (2011). "Behavior of fire-damaged mortar under variable heating and re-curing conditions." *ACI Materials Journal*, 108(3), 281-289.

Henry, M., Darma, I. S. and Sugiyama, T., (2014). "Analysis of the effect of heating and re-curing on the microstructure of high-strength concrete using X-ray CT." *Construction and Building Materials*, 67(a), 37-46.

Hoshen, J. and Kopelman, R., (1976). "Percolation and cluster distribution I. Cluster multiple labeling technique and critical concentration algorithm." *Physics Review B*, 14, 3438-3445.

Ikeda, S., Nakano, N. and Nakashima, Y., (2000). "Three-dimensional study on the interconnection and shape of crystals in a graphic granite by X-ray CT and image analysis." *Mineral Magazine*, 64(5), 945-959.

Khoury, G. A., (1992). "Compressive strength of concrete at high temperatures: a reassessment." *Magazine of Concrete Research*, 44(161), 291-309.

Landis, E. N. and Keane, D. T., (2010). "X-ray microtomography." *Materials Characterization*, 61, 1305-1316.

Lin, W. M., Lind, T.D. and Powers-Couche, L. J., (1996). "Microstructures of fire-damaged concrete." *ACI Materials Journal*, 93(3), 199-205.

Petzold, A. and Rohrs, M., (1970). "*Concrete for High Temperatures*." New York: Maclaren and Sons, Ltd.

Poon, C., Azhar, S., Anson, M. and Wong, Y. L., (2001). "Comparison of the strength and durability performance of normal and high strength pozzolanic concretes at elevated temperatures." *Cement and Concrete Research*, 31(9), 291-300.

Promentilla, M. A. B., Sugiyama, T., Hitomi, T., and Takeda, N., (2008). "Characterizing the 3D pore structure of hardened cement paste with synchrotron microtomography." *Journal of Advanced Concrete Technology*, 6(2), 273-286.

Promentilla, M. A. B. and Sugiyama, T., (2010). "X-ray microtomography of mortars exposed to freezing-thawing action." *Journal of Advanced Concrete Technology*, 8(2), 97-111.

Sarshar, R. and Khoury, G. A., (1993). "Material and environmental factors influencing the compressive strength of unsealed cement paste and concrete at high temperatures." *Magazine of Concrete Research*, 45(162), 51-61.

Taylor, H. F. W., (1997). "*Cement Chemistry*." London: Academic Press.

Tovey, A. K., (1970). "Assessment and repair of fire-damaged concrete structures – an update." In: T.Z. Harmathy (Ed.). *Evaluation and repair of fire damaged to concrete, ACI SP-92*. Farmington Hills: American Concrete Institute, 47-62.